PAPER IN FOREFRONT

Mass spectrometry imaging with high resolution in mass and space (HR^2 MSI) for reliable investigation of drug compound distributions on the cellular level

Andreas Römpp · Sabine Guenther · Zoltan Takats · Bernhard Spengler

Abstract Mass spectrometry (MS) imaging is a versatile method to analyze the spatial distribution of analytes in tissue sections. It provides unique features for the analysis of drug compounds in pharmacokinetic studies such as label-free detection and differentiation of compounds and metabolites. We have recently introduced a MS imaging method that combines high mass resolution and high spatial resolution in a single experiment, hence termed HR^2 MS imaging. In the present study, we applied this method to analyze the spatial distribution of the anti-cancer drugs imatinib and ifosfamide in individual mouse organs. The whole kidney of an animal dosed with imatinib was measured at 35 μm spatial resolution. Imatinib showed a well-defined distribution in the outer stripe of the outer medulla. This area was analyzed in more detail at 10 μm step size, which constitutes a tenfold increase in effective spatial resolution compared to previous studies of drug compounds. In parallel, ion images of phospholipids and heme were used to characterize the histological features of the tissue section and showed excellent agreement with histological staining of the kidney after MS imaging. Ifosfamide was analyzed in mouse kidney at 20 μm step size and was found to be accumulated in the inner medulla region. The identity of imatinib and ifosfamide was confirmed by on-tissue MS/MS measurements. All measurements including mass spectra from 10 μm pixels featured accurate mass (≤2 ppm root mean square) and mass resolving power of $R=30,000$. Selected ion images were generated with a bin size of $\Delta m/z=0.01$ ensuring highly specific information. The ability of the method to cover larger areas was demonstrated by imaging a compound in the intestinal tract of a rat whole-body tissue section at 200 μm step size. The described method represents a major improvement in terms of spatial resolution and specificity for the analysis of drug compounds in tissue sections.

Keywords Mass spectrometry imaging · Drug compounds · Accurate mass · High-resolution mass spectrometry

A. Römpp · S. Guenther · Z. Takats · B. Spengler (✉)
Institute of Inorganic and Analytical Chemistry,
Justus Liebig University,
Giessen, Germany
e-mail: bernhard.spengler@anorg.chemie.uni-giessen.de

Introduction

Mass spectrometry (MS) imaging has become a widely used analytical technique due to its ability to visualize the distribution of a large variety of analytes [1–5]. Numerous applications have been published including the imaging of lipids [6], peptides [7, 8], and proteins [9].

MS imaging has also been applied to detection of drug compounds [10, 11]. Its ability for label-free detection and differentiation between compound and metabolites are major advantages compared to autoradiography, which is the classical method to investigate the spatial distribution of drug candidates [12].

The spatial resolution of MS imaging measurements of drug compounds is typically in the range of 200 to 500 μm, which is sufficient to analyze whole-body sections [11, 13] or individual rat organs [14], but insufficient to resolve detailed features in mouse organs. The highest resolution reported so far for drug compounds was 100 μm [11, 15].

Mass analyzers employed are typically time-of-flight (TOF) systems such as QTOF [13], TOF/TOF [11, 15], or ion mobility TOF instruments [16]. The use of triple-quadrupole [17] and ion trap [18] mass spectrometers was also reported. Compounds are usually detected in MS/MS mode in order to increase the specificity of the measurement and to prevent interference of matrix cluster ions which are typically abundant in the low mass range [11]. Accurate mass measurements can be used for direct identification without the need for separate fragmentation of each analyte, in many cases. Mass spectrometers with mass accuracies in the low parts per million range were routinely used in many bioanalytical applications. The highest mass accuracy and mass resolution is obtained by Fourier transform (FT) ion cyclotron resonance mass spectrometers [19, 20]. Another type of FTMS is the recently introduced orbital trapping system [21]. The use of these high-quality mass analyzers in matrix-assisted laser desorption/ionization (MALDI) imaging is limited to very few examples so far [7, 22, 23]. These measurements showed, that the full complexity of biological samples can only be resolved with high mass accuracy and high mass resolution analyses. The only FTMS imaging measurement of drug compounds reported so far was performed at 350 μm spatial resolution [14].

Recently, we introduced a method combining for the first time the capabilities of FTMS with spatial resolution in the cellular range [23]. We termed this method HR^2 MS imaging because of its ability to obtain high resolution in mass and space. Analytes can be detected with sub-parts per million (ppm) mass accuracy, and MS/MS experiments can be performed in order to verify identification. The obtained MS images are highly specific and show excellent correlation to histological features on the cellular level. Applications include the analysis of phospholipids [23] and neuropeptides [24] at a spatial resolution of 5 μm. In the present study, we applied our method to the detection of the anticancer drugs imatinib and ifosfamide in mouse kidney sections. The resulting MS images provide detailed information on spatial distribution and represent the first mass spectrometric imaging analysis of drug compounds at 10 μm spatial resolution. This constitutes a tenfold increase in effective spatial resolution compared to previous studies and makes detailed histological feature in mouse organs accessible for the first time.

Experimental

Samples

Mouse tissue samples were obtained from Semmelweis University, Budapest, Hungary. CD1-nude mice (9 weeks old) received a single oral dose of 750 mg/kg imatinib and 375 mg/kg ifosfamide, respectively. Animals were sacrificed 2 h after administration by neck disruption. Kidneys were resected and immediately snap-frozen in liquid nitrogen. Tissue samples were cut in sections of 20 μm thickness with a cryotome (HM 525 cryostat, Thermo Scientific, Dreieich, Germany) at −20 °C. The sections were thaw-mounted on glass slides. The mounted samples were stored at −80 °C until analysis. For measurements, tissue sections were brought to room temperature in a desiccator (30 min) to avoid condensation of humidity on the sample surface. Optical images of tissue sections were taken before sample preparation with an Olympus BX-40 microscope (Olympus Europa GmbH, Hamburg, Germany). No washing steps were applied prior to matrix application. A solution of the matrix 2,5-dihydroxybenzoic acid (DHB; 98% purity, Aldrich, Germany) in concentrations of 30 mg/mL was prepared in acetone/water (0.1% TFA) 1:1 v/v. The matrix solution was applied with a specially designed pneumatic sprayer [25]. Tissue sections were analyzed immediately after matrix application. All required ethical permissions were obtained for the animal experiments from the respective institutional ethical committee.

Instrumentation

All experiments were performed using a home-built atmospheric pressure scanning microprobe MALDI (AP-SMALDI) imaging source attached to a linear ion trap/FT orbital trapping mass spectrometer (LTQ Orbitrap Discovery, Thermo Scientific GmbH, Bremen, Germany). The setup of the AP-SMALDI imaging source is given in detail elsewhere [26]. A nitrogen laser (λ=337 nm, LTB MNL-106, LTB, Berlin, Germany) operating at a repetition rate of 60 Hz was used for desorption/ionization in this study. The laser beam was focused by the centrally bored objective lens to an optical diameter of 8.4 μm (1/e^2 definition). The effective diameter of the ablation spot varies with chosen laser energy [27] and was always less than 10 μm for experiments with 10 μm pixel size. The laser was slightly defocused (and laser energy increased for compensation) for experiments with 20 and 35 μm pixel size in order to increase irradiation area and thus ion yield.

Ions from 30 laser pulses were accumulated in the linear ion trap for each mass spectrum. The target voltage was set to 4.3 kV. The step size of the sample stage was set to the desired pixel size (10, 20, 35, and 200 μm).

The LTQ Orbitrap instrument was operated in positive-ion mode and in the normal mass range mode (m/z=100–1,000). MS imaging measurements were performed using the Orbitrap detector with a mass resolving power of 30,000 at m/z= 400 in profile mode (i.e., mass peaks were not centroided for data reduction). Automatic gain control (AGC) was disabled during the measurement, and ion injection time was

manually set to 650 ms. A mass accuracy of <2 ppm was achieved by internal calibration using the lock mass feature of the instrument. Cycle times of the ion trap/Orbitrap system were 1.3 s (including stage movement).

Data processing

Selected ion images were generated using the software package MIRION developed in-house. The imaging software imports raw data files as stored by the LTQ Orbitrap instrument software during image acquisition and couples this mass spectrometric information with additional scanning metadata, stored in separate data files by our ion source control program. This metadata includes the number of lines and columns of the image and the pixel size. Raw data files consist of linear ion trap or FT mass spectra. The imaging software is able to create ion images from any of the detected mass-to-charge values with any selected mass window (bin width). A fast image browser of the MIRION software assists in selecting of images. In this work, ion images of selected mass-to-charge values were created from the FTMS data set with a bin width of $\Delta m/z=0.01$. Intensity values in ion images were normalized to the highest intensity measured for each ion species separately. Up to three different ion images were overlayed in RGB images by the software to display different ion species in parallel. No other post-processing steps such as interpolation or normalization to matrix signals were applied to the images.

Results and discussion

The distribution of imatinib and ifosfamide in mouse kidney sections was analyzed. The kidney is the most important organ for elimination of drug compounds and other xenobiotics from the body. The mouse kidney consists of three main regions: cortex, medulla, and pelvis. The medulla is subdivided into the inner and the outer medulla. The outer medulla is further differentiated in outer and inner stripe. Three main processes affect the elimination of a compound in the kidney: (1) filtration from the blood circulation into the primary urine which occurs in the glomeruli of the kidney's nephrons (located in the cortex), (2) reabsorption from the primary urine into the blood circulation by active transport processes, and (3) additional secretion of the compound from the blood circulation into the urine. Both processes (reabsorption and additional secretion) occur in the tubules of the kidney's nephrons (located in cortex and outer and inner medulla).

Imatinib is a drug used for the treatment of different cancer types such as chronic myelogenous leukemia and gastrointestinal stromal tumors. The distribution of this compound in mouse kidney was analyzed at two different settings of spatial resolution. Figure 1A shows an overlay of selected ion images from several phospholipids in the mouse kidney as measured by MALDI MS imaging with a lateral resolution of 35 μm. The distribution of these phospholipids corresponds very well to histological features of the kidney as determined by H&E staining (Fig. 1C). The cortex is represented in Fig. 1A by the potassium adduct of the phospholipid PC(32:0) in green. The outer stripe of the outer medulla is represented by the potassium adduct of the phospholipid PC(40:6) colored in blue, and the inner stripe of the outer medulla is represented by potassium adduct of the phospholipid PC(38:5) in red. Additional histological features such as the inner medulla and renal sinus can also be clearly identified by their lipid composition. Examples of several selected ion images are shown in the Supplementary Material (Figure S1). Blood vessels can be identified by the selected ion image of the heme b group (Supplementary Material Figure S2). High intensities of the heme signal were also detected in the glomeruli, which are about 100 μm in diameter. The glomeruli are spread out in the cortex of the mouse kidney. They filter compounds from the blood stream and therefore express high blood circulation.

The distribution of the drug compound imatinib in the mouse kidney is shown Fig. 1B. Imatinib ([M+H]$^+$, $m/z=$ 494.2662) is colored in green, while two phospholipids are included to indicate the histological structure of the kidney. The cortex is shown by the phospholipid PC(32:0) colored in red; the medulla, papilla, and sinus are shown by the phospholipid PC(34:1) colored in blue. All ion images were generated with a bin width of $\Delta m/z=0.01$, e.g., $m/z=$ 494.260–494.270 for imatinib. Figure 1D shows an Orbitrap mass spectrum of imatinib obtained from a single pixel (sample position). The molecular ion peak of imatinib was detected with a mass deviation of −0.4 ppm and a mass resolving power of $R=30,000$ in this spectrum. The overall mass accuracy for imatinib in the imaging measurement calculated from 5,862 individual spectra was 2 ppm root mean square (RMS). This high mass accuracy allows for confident identification of the imaged compound. The identity of imatinib was additionally verified via on-tissue MS/MS measurements. The MS/MS spectrum showed the expected and characteristic fragmentation pattern of imatinib (Supplementary Material Figure S3).

Selected ion images of phospholipids and heme provide detailed information on the structure of the tissue section. Identification of tissue types, which can otherwise only be achieved by close examination of the H&E stained section by a trained histologist, is easily possible based on the MS imaging data. This information can be used to determine the exact location of the target analyte (imatinib in this case) in the mouse kidney. The colocalization of imatinib and PC(40:6) (Fig. 1A, blue) indicates that imatinib is
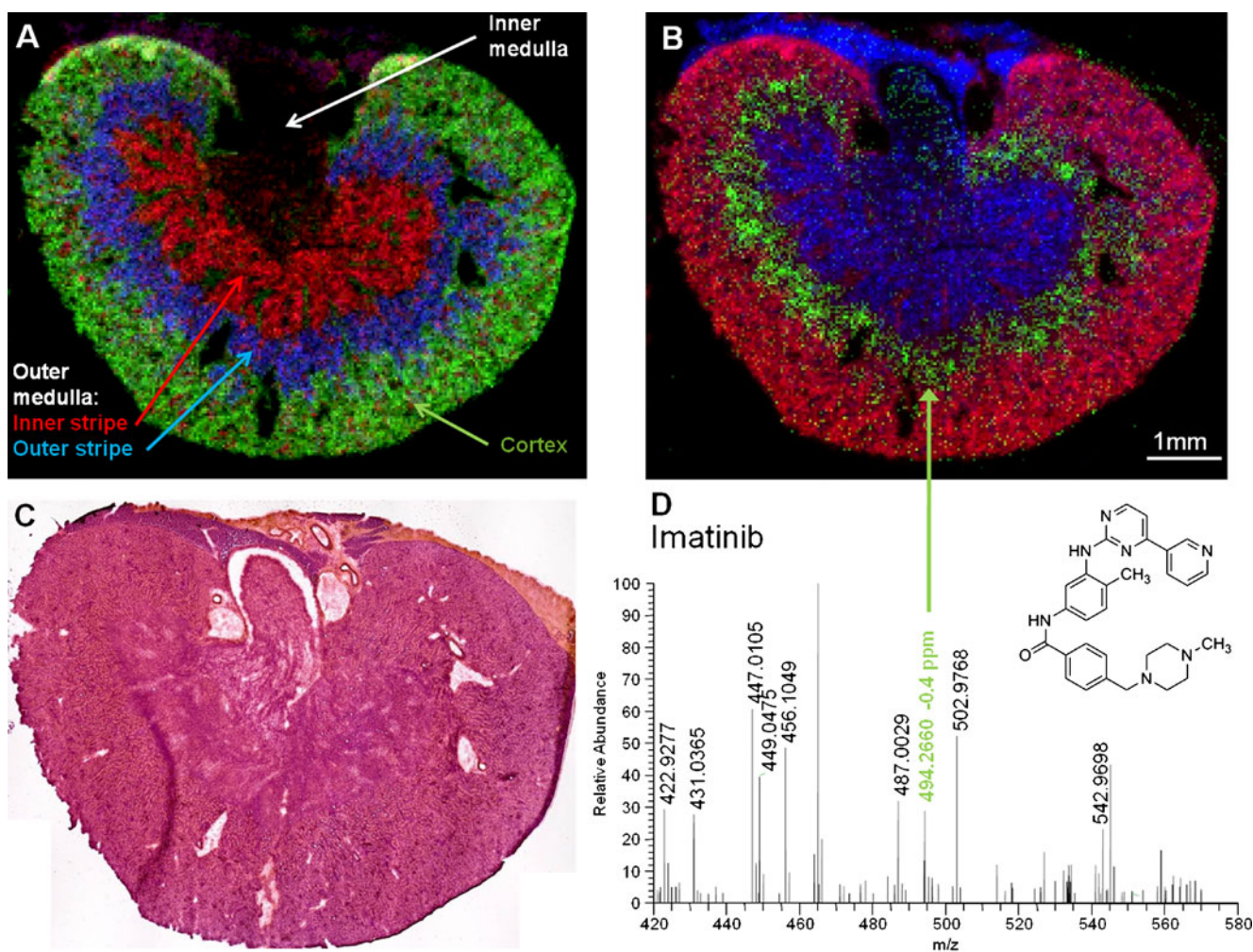
Fig. 1 **A** Overlay of selected ion images: *green*, [PC(32:0)+K]$^+$= 772.5253 cortex; *blue*, [PC(40:6)+K]$^+$=872.5566 outer stripe outer medulla; and *red*, [PC(38:5)+K]$^+$=846.5410 inner stripe outer medulla; FTMS image, 225×150 pixels; 35 μm step size; bin width, $\Delta m/z$=0.01. **B** Overlay of selected ion images: *red*, [PC(32:0)+K]$^+$=772.5253; *green*, imatinib [M+H]$^+$=494.2662; and *blue*, [PC(34:1)+H]$^+$= 760.5851; FTMS image, 225×150 pixels; 35 μm step size; bin width, $\Delta m/z$=0.01. **C** Optical image of the investigated mouse kidney section; H&E stained after MS imaging measurement. **D** Single-pixel FTMS spectrum of the outer stripe outer medulla of the mouse kidney section

present in the outer stripe of the outer medulla. In order to investigate this region in more detail, a second experiment on an adjacent kidney section was performed with a step size of 10 μm.

Selected ion images of phospholipids and heme are shown in Fig. 2A. The potassium adduct of SC(16:0) (m/z= 741.5307) representing the outer stripe of the outer medulla is shown in green. The protonated ion of PC(34:1) shown in blue represents the inner stripe of the outer medulla. Blood vessels are indicated by the heme b signal shown in red.

Figure 2C displays the optical image of the investigated part of the kidney section after MS imaging analysis and H&E staining. The outer stripe of the outer medulla is clearly distinguishable from the inner stripe of the outer medulla by its highly structured features (upper edge of the optical image) compared to the rather smooth tissue of the inner stripe of outer medulla. The large capillary in the

upper right corner of the optical image is the renal vein, which removes the blood from the kidney. The bright dots in the inner stripe of the outer medulla are called vasa recta. The blood vessels propagate from outer medulla into the inner medulla and reverse. They are necessary for processes like reabsorption and secretion which occur in the tubules of the kidney's nephrons. The localization of the heme signal in the MS imaging experiment (Fig. 2A, red) corresponds well to the topology of the blood vessels. Both vasa recta and renal vein are clearly visible in the mass spectrometric image. Figure 2B shows the distribution of imatinib (shown in green) in the mouse kidney. The high-resolution image confirms the specific location of imatinib in the outer stripe of the outer medulla.

Figure 2D shows a FT mass spectrum of imatinib from a single 10 μm pixel. Imatinib was detected in this mass spectrum with a mass deviation of −0.2 ppm. The overall

Fig. 2 **A** Overlay of selected ion images: *green*, [SC(16:0)+K]$^+$= 741.5307 outer stripe outer medulla; *blue*, [PC(34:1)+H]$^+$= 760.5851 inner stripe outer medulla; and *red*, [heme b]$^+$= 616.1767 vasa recta; FTMS image, 150×203 pixels; 10 μm step size; bin width Δm/z=0.01. **B** Overlay of selected ion images: *green*, imatinib [M+H]$^+$= 494.2662 outer stripe outer medulla; *blue*, [PC(38:5)+K]$^+$= 846.5410 inner stripe outer medulla; and *red*, [heme b]$^+$= 616.1767 vasa recta; FTMS image, 150×203 pixels; 10 μm step size; bin width Δm/z=0.01. **C** Optical image of the investigated mouse kidney section; H&E stained after the MS imaging measurement. **D** Single-pixel FTMS spectrum of the outer stripe outer medulla of mouse kidney section
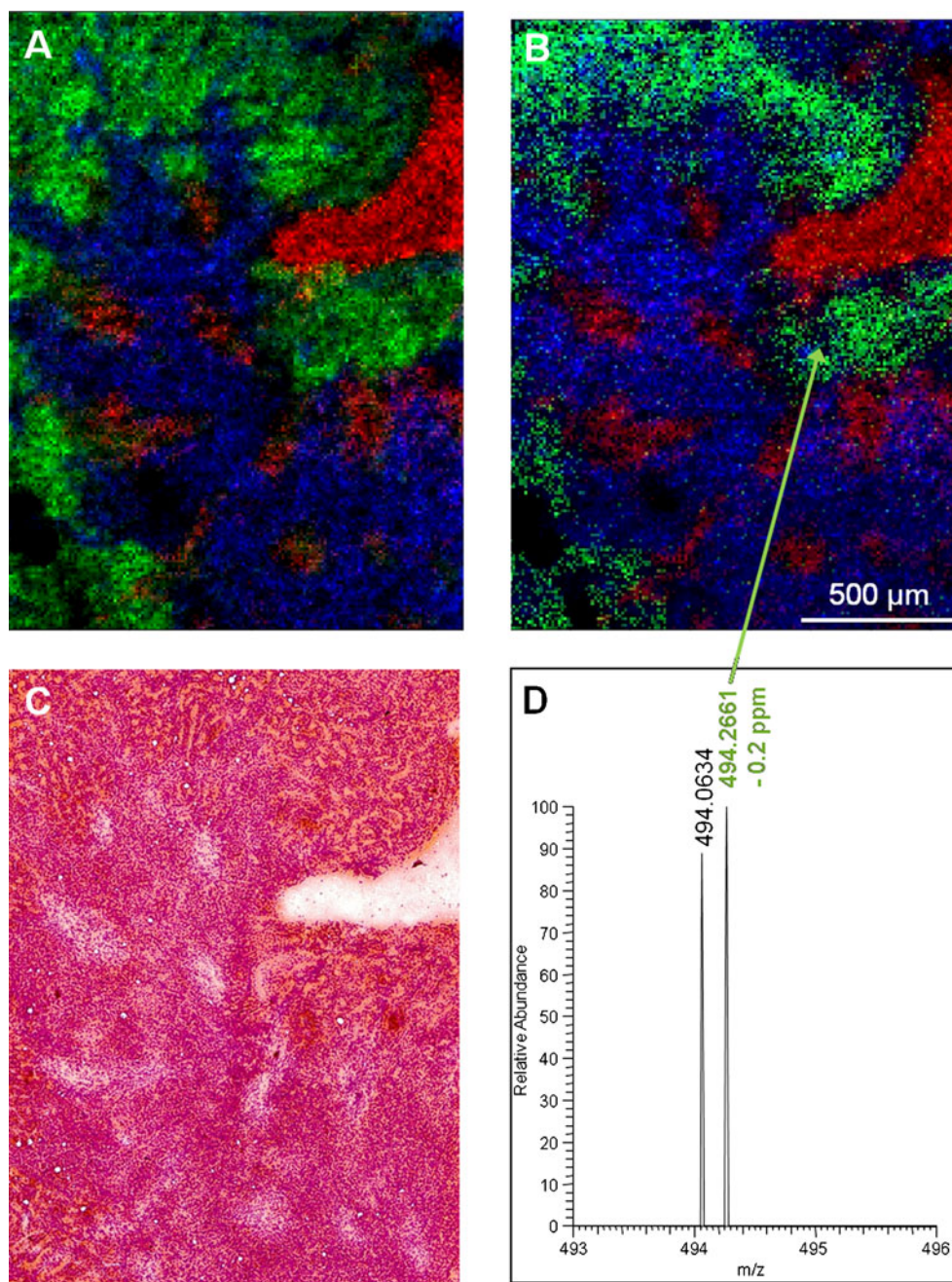
mass accuracy of the imaging measurement for imatinib was 1.8 ppm RMS (calculated from 5,816 individual spectra), which is remarkable considering that the number of ions generated from a sample area of 10 μm diameter is rather low. The mass spectrum also demonstrates the benefit of high mass resolving power. The two mass peaks shown in the mass spectrum Fig. 2D would not be separated if the MS measurement was performed with low mass resolving power. The corresponding ion image would instead show an overlay of the distributions of the two signals and not the specific distribution of the drug compound. Even with high mass resolving power this would happen if the image bin width were not chosen

appropriately. If the measurement is performed with high mass resolution, but the ion image bin width is set to Δm/z=1 (for example), then the benefit from the highly resolved MS measurements is lost, since the resulting ion image shows an overlay of all signals within the mass window of Δm/z=1 and not only the distribution of the desired compound (see Supplementary Material Figure S4 for comparison).

Ion images of the 10 μm measurements also show excellent correlation with the histological features of the mouse kidney. The localization of imatinib in the outer stripe of the outer medulla was confirmed by this additional measurement. This region consists mainly of the tubules of
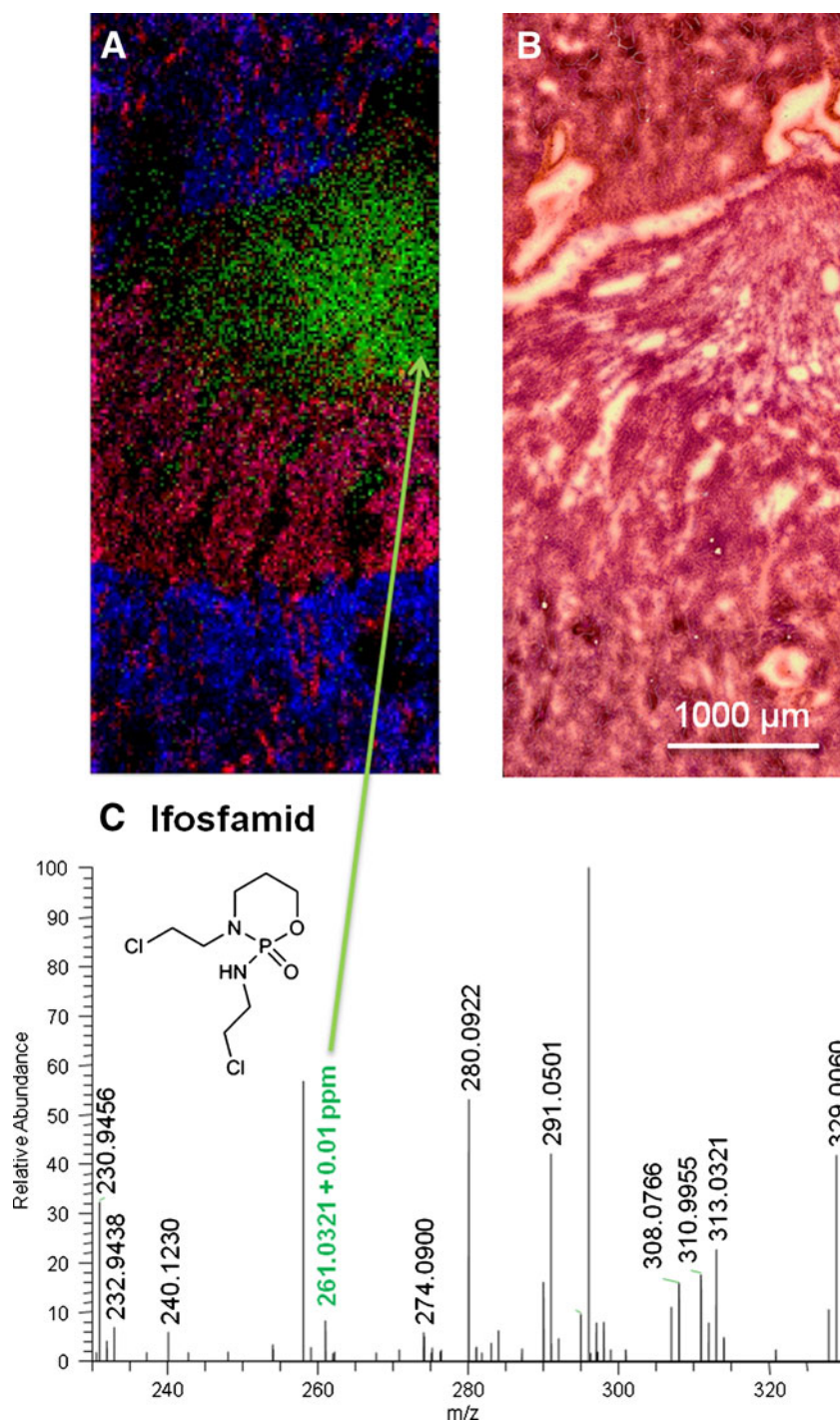
the kidney's nephrons, which are responsible for reabsorption/additional secretion processes of endogenous compounds and exogenous compounds (pharmaceuticals) from the urine into the blood circulation and reverse. The well-defined distribution of imatinib in the outer medulla region can tentatively be associated with the selective accumulation of drug molecules in the so-called proximal tubules. Imatinib is a strong inhibitor of tyrosin kinases, which are known to show distinct distributions in the glomeruli and

the proximal tubules, respectively [28]. A more detailed analysis of the causes would require a dedicated study with a higher number of samples. Ion suppression effects, which are a highly debated issue in MS imaging, do not seem to be responsible for the reported spatial distribution. MS images in this study were not normalized or otherwise modified after acquisition. Normalization to the total ion current (TIC) is a common method to account for ion suppression effects on tissue. However, in our experiment,

the TIC signal was homogeneous over the whole tissue section, and normalization did not lead to any significant change in signal distribution as can be seen in Supplementary Material Figure S5. Consequently, ion suppression does not seem to be a major problem in this experiment. MS images were also not interpolated, smoothed, or digitally filtered, in order to show the quality of the original data. Raw images are highly informative and reliable due to a high pixel coverage and large number of acquired pixels. Interpolation or other image processing steps do not result in higher quality of image information but may create artifacts. Original and interpolated MS images are given in Supplementary Material Figure S6 for comparison.

The time demand of our method is comparable to that of standard MALDI-TOF systems at 1.3 s per pixel. This time is averaged over the complete image and includes stage movement, MS detection, and on-the-fly internal calibration of mass spectra. MALDI imaging experiments can also be performed at 5 μm pixel size as demonstrated for phospholipids and neuropeptides [23, 24]. An important factor for achievable spatial resolution is limit of detection of the mass spectrometer. Applicability of 5 μm pixel size to drug compound imaging will be evaluated in future experiments.

In addition to imatinib, the distribution of another anticancer drug, ifosfamide, was analyzed in mouse kidney. Its distribution in the kidney 2 h after administration was investigated by MS imaging with a lateral resolution of 20 μm. Figure 3A shows the distribution of ifosfamide ($[M+H]^+$, $m/z=261.0321$) in the mouse kidney as determined by MS imaging (green). The cortex tissue is represented by the potassium adduct of phospholipid PC(38:4) shown in blue, and the outer medulla is represented by the potassium adduct of phospholipid PC(38:6) shown in red. Figure 3B displays the analyzed tissue section after MS imaging analysis and H&E staining. Three different tissue types are visible in Fig. 3B. Starting from top to bottom, cortex is followed by inner medulla, outer medulla, and cortex again. An image of the whole tissue section after H&E staining is shown in Supplementary Material Figure S7. As can be seen by comparison of Fig. 3A, B, ifosfamide is mainly detected in the inner medulla (green).

Figure 3C shows a single-pixel FT mass spectrum of ifosfamide from the imaging measurement. Ifosfamide was detected with a mass deviation of +0.8 ppm in this spectrum. Mass accuracy for the whole imaging measurement was 1.4 ppm RMS (calculated from 3,952 individual spectra) for ifosfamide. The identity of ifosfamide was also verified via on-tissue MS/MS measurements. The MS/MS spectrum showed the characteristic fragmentation pattern for ifosfamide (Supplementary Material Figure S8).

Ifosfamide was mainly detected in the inner medulla. Unlike imatinib, ifosfamide is not a molecularly targeted drug; it specifically alkylates nucleic acids, hindering protein expression and cell proliferation this way. Detection of the molecule in the inner medulla can tentatively be associated to increased accumulation in this tissue due to its lipophilic properties. Again, ion suppression as determined by TIC distribution evaluation was not relevant for this measurement.

Our technique is not only able to obtain highly specific information at high spatial resolution but it can also be used to analyze larger specimen, including whole-body tissue sections from rodents. Figure 4 shows a measurement of the intestinal tract of a whole rat section covering an area of
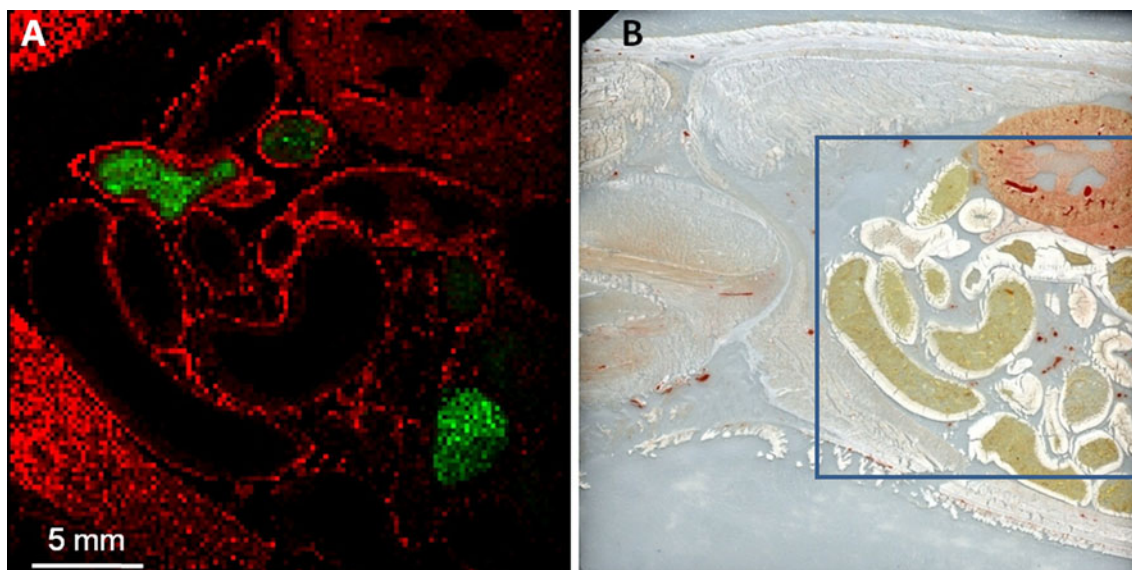
Fig. 4 **A** Overlay of selected ion images: *red*, $[SC(18:0)+K]^+=769.5620$; *green*, administered compound; FTMS image, 128×150 pixels; 200 μm step size; bin width $\Delta m/z=0.01$. **B** Optical image of the investigated rat whole-body section; *blue square* indicates the measured area

3×2.5 cm at 200 μm pixel size. The selected ion images (Fig. 4A) show the phospholipid SC(18:0) (red), which gives a good indication of the histological features of the tissue section (see Fig. 4B for comparison) and an orally administered compound (green). The molecular images show the distribution of the compound in distinct areas, information which could already be used to provide a pharmacokinetic profile. Furthermore, the analysis of a whole-body section could be used to direct scans to be acquired with high spatial resolution. For example, detailed data on the uptake and/or excretion of the compound and its metabolites through the stomach and intestinal walls could be obtained (compare Figure S9). This is typically not possible with a commercial setup due to limitations in laser spot size and sample preparation. Obviously, while it would be possible to acquire data from the full rat section at high resolution, this would require days of acquisition time and is hardly feasible. However, the combination of an overview scan with a zoom scan delivers a good compromise between acquisition time and spatial information.

Conclusions

In this work, we present for the first time analysis of drug compounds at 10 μm effective spatial resolution by MS imaging. Our method allows for the analysis of the compound distribution in a mouse organ with a richness in detail that was not accessible with previous methods. At the same time, the method provides detailed information on histological features based on the distribution of phospholipids and other endogenous compounds. Correlation of these different images allows for fast and easy interpretation of the drug compound distribution, and areas of accumulation can be directly linked to certain tissue types. The measurements feature high mass accuracy and high mass resolving power, allowing for reliable identification of the imaged compounds. Identification can be confirmed by on-tissue MS/MS experiments. The generated MS images are highly specific because they represent a very narrow mass range ($\Delta m/z = 0.01$), preventing interference with neighboring peaks. This ensures that the generated ion images represent the distribution of the targeted compound with high certainty. We demonstrated that the method can also be used for analysis of larger specimen such as rat whole-body tissue sections. Measurement speed of our method is comparable to standard MALDI-QTOF measurements, and thus does not pose any practical limitations on study design.

The combination of these features in a single experiment results in unprecedented depth and quality of information that can be exploited in pharmaceutical studies, as well as in other bioanalytical applications.

References

1. Chughtai K, Heeren RMA (2010) Mass spectrometric imaging for biomedical tissue analysis. Chem Rev 110(5):3237–3277
2. McDonnell LA, Heeren RMA (2007) Imaging mass spectrometry. Mass Spectrom Rev 26(4):606–643. doi:10.1002/mas.20124
3. Spengler B, Hubert M (2002) Scanning microprobe matrix-assisted laser desorption ionization (SMALDI) mass spectrometry: instrumentation for sub-micrometer resolved LDI and MALDI surface analysis. J Am Soc Mass Spectrom 13(6):735–748
4. Spengler B, Hubert M, Kaufmann R (1994) MALDI ion imaging and biological ion imaging with a new scanning UV-laser microprobe. In: Proceedings of the 42nd Annual Conference on Mass Spectrometry and Allied Topics, Chicago, Illinois, 29 May–3 June, p 1041
5. Stoeckli M, Chaurand P, Hallahan DE, Caprioli RM (2001) Imaging mass spectrometry: a new technology for the analysis of protein expression in mammalian tissues. Nat Med 7(4):493–496
6. Jackson SN, Wang HYJ, Woods AS (2005) In situ structural characterization of phosphatidylcholines in brain tissue using MALDI-MS/MS. J Am Soc Mass Spectrom 16(12):2052–2056. doi:10.1016/j.jasms.2005.08.014
7. Chen RB, Jiang XY, Conaway MCP, Mohtashemi I, Hui LM, Viner R, Li LJ (2010) Mass spectral analysis of neuropeptide expression and distribution in the nervous system of the lobster *Homarus americanus*. J Proteome Res 9(2):818–832. doi:10.1021/pr900736t
8. Stoeckli M, Staab D, Staufenbiel M, Wiederhold KH, Signor L (2002) Molecular imaging of amyloid beta peptides in mouse brain sections using mass spectrometry. Anal Biochem 311(1):33–39
9. Reyzer ML, Caprioli RM (2007) MALDI-MS-based imaging of small molecules and proteins in tissues. Curr Opin Chem Biol 11(1):29–35. doi:10.1016/j.cbpa.2006.11.035
10. Reyzer ML, Hsieh YS, Ng K, Korfmacher WA, Caprioli RM (2003) Direct analysis of drug candidates in tissue by matrix-assisted laser desorption/ionization mass spectrometry. J Mass Spectrom 38(10):1081–1092. doi:10.1002/jms.525
11. Stoeckli M, Staab D, Schweitzer A (2007) Compound and metabolite distribution measured by MALDI mass spectrometric imaging in whole-body tissue sections. Int J Mass Spectrom 260(2–3):195–202. doi:10.1016/j.ijms.2006.10.007
12. Solon EG, Schweitzer A, Stoeckli M, Prideaux B (2010) Autoradiography, MALDI-MS, and SIMS-MS imaging in pharmaceutical discovery and development. AAPS J 12(1):11–26. doi:10.1208/s12248-009-9158-4
13. Khatib-Shahidi S, Andersson M, Herman JL, Gillespie TA, Caprioli RM (2006) Direct molecular analysis of whole-body animal tissue sections by imaging MALDI mass spectrometry. Anal Chem 78(18):6448–6456. doi:10.1021/ac060788p
14. Cornett DS, Frappier SL, Caprioli RM (2008) MALDI-FTICR imaging mass spectrometry of drugs and metabolites in tissue. Anal Chem 80(14):5648–5653. doi:10.1021/ac800617s
15. Acquadro E, Cabella C, Ghiani S, Miragoli L, Bucci EM, Corpillo D (2009) Matrix-assisted laser desorption ionization imaging mass spectrometry detection of a magnetic resonance imaging contrast agent in mouse liver. Anal Chem 81(7):2779–2784. doi:10.1021/ac900038y

16. Trim PJ, Henson CM, Avery JL, McEwen A, Snel MF, Claude E, Marshall PS, West A, Princivalle AP, Clench MR (2008) Matrix-assisted laser desorption/ionization-ion mobility separation-mass spectrometry imaging of Vinblastine in whole body tissue sections. Anal Chem 80(22):8628–8634. doi:10.1021/ac8015467

17. Hopfgartner G, Varesio E, Stoeckli M (2009) Matrix-assisted laser desorption/ionization mass spectrometric imaging of complete rat sections using a triple quadrupole linear ion trap. Rapid Commun Mass Spectrom 23(6):733–736. doi:10.1002/rcm.3934

18. Drexler DM, Garrett TJ, Cantone JL, Diters RW, Mitroka JG, Prieto Conaway MC, Adams SP, Yost RA, Sanders M (2007) Utility of imaging mass spectrometry (IMS) by matrix-assisted laser desorption ionization (MALDI) on an ion trap mass spectrometer in the analysis of drugs and metabolites in biological tissues. J Pharmacol Toxicol Meth 55(3):279–288. doi:10.1016/j.vascn.2006.11.004

19. Marshall AG, Hendrickson CL (2002) Fourier transform ion cyclotron resonance detection: principles and experimental configurations. Int J Mass Spectrom 215(1–3):59–75

20. Römpp A, Taban IM, Mihalca R, Duursma MC, Mize TH, McDonnell LA, Heeren RMA (2005) Examples of Fourier transform ion cyclotron resonance mass spectrometry developments: from ion physics to remote access biochemical mass spectrometry. Eur J Mass Spectrom 11(5):443–456

21. Scigelova M, Makarov A (2006) Orbitrap mass analyzer—overview and applications in proteomics. Proteomics 6(1):16–21. doi:10.1002/pmic.200600528

22. Landgraf RR, Conaway MCP, Garrett TJ, Stacpoole PW, Yost RA (2009) Imaging of lipids in spinal cord using intermediate pressure matrix-assisted laser desorption-linear ion trap/Orbitrap MS. Anal Chem 81(20):8488–8495. doi:10.1021/ac901387u

23. Römpp A, Guenther S, Schober Y, Schulz O, Takats Z, Kummer W, Spengler B (2010) Histology by mass spectrometry: label-free tissue characterization obtained from high-accuracy bioanalytical imaging. Angew Chem Int Ed 49 (22):3834–3838

24. Guenther S, Römpp A, Kummer W, Spengler B (2011) AP-MALDI imaging of neuropeptides in mouse pituitary gland with 5 μm spatial resolution and high mass accuracy. Int J Mass Spectrom. doi:10.1016/j.ijms.2010.11.011

25. Bouschen W, Schulz O, Eikel D, Spengler B (2010) Matrix vapor deposition/recrystallization and dedicated spray preparation for high-resolution scanning microprobe matrix-assisted laser desorption/ionization imaging mass spectrometry (SMALDI-MS) of tissue and single cells. Rapid Commun Mass Spectrom 24 (3):355–364

26. Koestler M, Kirsch D, Hester A, Leisner A, Guenther S, Spengler B (2008) A high-resolution scanning microprobe matrix-assisted laser desorption/ionization ion source for imaging analysis on an ion trap/Fourier transform ion cyclotron resonance mass spectrometer. Rapid Commun Mass Spectrom 22(20):3275–3285. doi:10.1002/rcm.3733

27. Guenther S, Koestler M, Schulz O, Spengler B (2010) Laser spot size and laser power dependence of ion formation in high resolution MALDI imaging. Int J Mass Spectrom 294(1):7–15. doi:10.1016/j.ijms.2010.03.014

28. Weinman EJ, Lakkis J, Akom M, Wali RK, Drachenberg CB, Coleman RA, Wade JB (2002) Expression of NHERF-1, NHERF-2, PDGFR-alpha, and PDGFR-beta in normal human kidneys and in renal transplant rejection. Pathobiology 70(6):314–323. doi:10.1159/000071271